

DISCLAIMER

This report was prepared as an account of work sponsored by an agency of the United States Government. Neither the United States Government nor any agency thereof, nor any of their employees, makes any warranty, express or implied, or assumes any legal liability or responsibility for the accuracy, completeness, or usefulness of any information, apparatus, product, or process disclosed, or represents that its use would not infringe privately owned rights. Reference herein to any specific commercial product, process, or service by trade name, trademark, manufacturer, or otherwise does not necessarily constitute or imply its endorsement, recommendation, or favoring by the United States Government or any agency thereof. The views and opinions of authors expressed herein do not necessarily state or reflect those of the United States Government or any agency thereof.

PPPL--2571

DE89 004632

RF SHEATHS AND IMPURITY GENERATION BY ICRF ANTENNAS

F. W. Perkins

Princeton Plasma Physics Laboratory

P.O. Box 451

Princeton, New Jersey 08543

ABSTRACT

In general, Faraday screen elements in an ICRF antenna are not aligned precisely along the combined toroidal and poloidal magnetic fields. When plasma of density $n > 2\epsilon_0 V/eg^2 \sim 10^9 \text{ cm}^{-3}$ is present in the gap between elements, electron response to the parallel electric field shorts out the electric field over most of the gap, leaving a narrow sheath of positive space charge and intense electric field. Here V denotes the voltage across the gap and g the gap spacing. This intense electric field accelerates ions up to an appreciable fraction of the gap voltage ($\sim 1 \text{ kV}$), sufficient to cause physical sputtering of the screen material. Impurities so generated constitute the principal limitation on power density (kW/cm^2) for ICRF antennas. ICRF antenna and Faraday screen design principles which minimize sputtering are discussed.

1. INTRODUCTION

Heating by waves in the ion cyclotron range of frequencies (ICRF) has become the preferred auxiliary heating method for compact ignition experiments [1] on the basis of its experimental successes in large tokamaks [2-6] and available, low-cost technology [7]. But ICRF heating has detrimental effects as well, among them generation of metallic impurities from the Faraday screen material [8-10] and an increased influx of both hydrogen isotopes and carbon from graphite walls [10,11]. Can ICRF antennas be designed to ameliorate these effects?

A more specific question is: What are the limits of ICRF heating, especially in terms of the power density (in kilowatts/cm²) which can be transmitted through a Faraday screen? Present experiments [4] operate at roughly the 1 kW/cm² level. Could this be increased to 10 kW/cm²? Experiments have identified three classes of phenomena which potentially limit power density of ICRF antennas: (1) electrical breakdown, (2) increased hydrogen and carbon influx, and (3) metallic impurity release at the Faraday screens. This paper argues that electrical breakdown and hydrogen/carbon influx need not constrain power density, at least to the 10 kW/cm² level. The key limitation is impurity generation by rf sheaths which arise because the Faraday screen elements are not precisely aligned along the combined toroidal and poloidal magnetic field. If the argument is valid, then impurity generation at the screen can be minimized by appropriate design.

Electrical breakdown was addressed by Perkins and Kluge [12] in a study of resonant cavity antennas for Doublet-IIID. At the 10 kW/cm² level, elec-

tric fields did not exceed 9 kV/cm along the magnetic field, 50 kV/cm across the magnetic field, and 2.2 kV/cm at a vacuum-insulator interface in coaxial transmission lines. All these values were shown to be safely below conservative electrical breakdown criteria. The design utilized magnetic insulation by the toroidal field, non-standard capacitors, and non-standard rectangular coaxial transmission lines. Since none of these essential features were retained in the TFTR resonant cavity antenna [13], its breakdown voltage is reported to be below the 100 kV level computed for the DIII-D antenna. With sufficient care and support to fabricate special capacitors and transmission lines, electrical breakdown should not limit power density to below 10 kW/cm².

Recent data from JET [14] support the picture that enhanced particle flux from the walls is a global phenomena. Langmuir probes mounted in the belt limiters showed the plasma to be toroidally symmetric. ICRF-heating-induced density increases and profile flattening in the plasma scrape-off layer were observed only outside the region between the belt limiters. Density profiles between the belt limiters, where the ICRF antennas are located, showed little change. On the basis of these data, one can conclude that particle influx depends on total ICRF power, but not on antenna power density.

It follows that impurity generation from Faraday screens is the key phenomena limiting power density of an ICRF antenna. Experimental studies have shown that metallic impurity generation occurs only when the antenna is driven [10,15]. Furthermore, impurity generation must originate from phys-

ical sputtering because neutral atoms require several eV of energy to cross the scrape-off layer without ionization. Sputtering data [16-18] show that deuteron energies in the range of 100 eV-1 keV produce the maximum yield of ~ 0.04 atom/ion. On the other hand, electron temperatures in the scrape-off layer are measured to be $T_e \sim 20$ eV [11]—insufficient to cause appreciable sputtering if one assumes $T_i = T_e$.

Test stand experiments at Oak Ridge have demonstrated that energizing an rf antenna increased sputtering of a graphite-covered Faraday screen [19]. In recent JET experiments [20], a strong correlation between misalignment angle and metallic impurity generation was found, in contrast to earlier work on TFTR [21]. The simple theoretical picture developed in this paper supports the JET observations that misalignment angle plays a crucial role.

2. RF SHEATHS

How do deuterons acquire the energy required for physical sputtering? The thesis of this paper is that an rf sheath effect, which arises because Faraday screen elements are not precisely aligned along the combined poloidal and toroidal magnetic field, effectively narrows the gap between Faraday shield elements, thereby increasing the electric fields and accelerating ions up to an appreciable fraction of the gap voltage, which is roughly 1 kV/gap for TFTR and JET antennas.

Figure 1 shows a representative ICRF antenna configuration. Almost all the magnetic field lines which encircle the driven current strap also pass through one side of a Faraday screen slot and return through the other. For

our purposes, one can model the z -dependence of B_z by a sinusoid

$$B_z = \frac{\Phi k_0}{g} \sin(k_0 z) \cos(\omega t), \quad (1)$$

where

$$k_0 = \pi/l, \quad g = \text{gap distance}, \quad \Phi = \text{rf magnetic flux}. \quad (2)$$

A loop integral around the contour ABCDA shows that the time-varying rf magnetic flux induces a voltage

$$V = \omega \Phi \cos(k_0 z) \sin \omega t = \int_A^B \mathbf{E}_v \cdot d\mathbf{l} \quad (3)$$

across the gap. Usually, currents in the plasma and Faraday screen elements do not appreciably alter Eq. (3). Of course, some effect occurs. It is known as magnetic shielding [22,23] and Faraday screen designs minimize it. For our purposes, the rf flux which passes through the Faraday screen is well-approximated by the magnetic flux linked by the antenna current strap. Consequently,

$$V = V_{\text{ant}} \cos(k_0 z)/N, \quad (4)$$

where $V_{\text{ant}} \approx 50 - 100$ kV is the (largely reactive) voltage of the antenna and $N \approx 50$ is the number of Faraday screen slots. For the purposes of sheath theory, one takes the voltage V across the gap to be prescribed and computes the reaction of the sheath plasma to this voltage.

In most tokamak installations, Faraday screen elements point in the toroidal direction and the misalignment angle between the screen element direction and the magnetic field is

$$\theta = \frac{B_\theta}{B_T} = \frac{a}{Rq} \approx 0.1. \quad (5)$$

In JET, screen elements are tilted at $\theta_0 \approx 0.25$. The difference $\theta_0 - \theta \approx 0.15$ is comparable to Eq. (5). Figure ??b sketches a representative Faraday screen design. The element length l satisfies $l \gg g/\theta$, so the voltage V in Eq. (3) varies little over the z -distance traveled by a magnetic field line in traversing the gap. Let us therefore idealize the rf sheath problem to one-dimensional geometry and take the electron motion to be along magnetic field lines

$$m_e \frac{dv_{||}}{dt} = \theta e E_y, \quad \frac{dy}{dt} = \theta v_{||} = v_y. \quad (6)$$

Hence electrons have an effective mass for y -motion $m^* = m_e/\theta^2$.

Next, note two points: (1) The effective electron mass is still much less than the deuteron mass. (2) The electron plasma frequency ν_p^* , based on the effective mass, exceeds ICRF frequencies for reasonable estimates of the gap density ($n \gtrsim 10^{10} \text{ cm}^{-3}$)

$$\nu_p^* = (900 \text{ MHz}) \theta \left(\frac{n}{10^{10} \text{ cm}^{-3}} \right)^{1/2} \approx 90 \text{ MHz} \left(\frac{n}{10^{10} \text{ cm}^{-3}} \right)^{1/2}. \quad (7)$$

Thus electrons will travel rapidly along field lines and shield out the impressed electric field over most of the gap. This leaves a region of positive space charge and intense electric field near the negative potential boundary.

What electric field intensities will arise in the space charge region? An immobile ion model gives a useful estimate. Figure ?? portrays the situation when the electric field is in the negative y -direction. The space charge region is $0 < y < d$, and the electric field must vanish at $y = d$

$$E = \begin{cases} 0, & y > d, \\ ne(y - d)/\epsilon_0, & y < d. \end{cases} \quad (8)$$

The potential drop V_g across the gap is determined by Eq. (3), which, in turn, determines d via

$$-\int_0^d E dy = \frac{n e d^2}{2 \epsilon_0} = V_g. \quad (9)$$

Note that d is the Debye length at a "temperature" $T_e = 2eV_g$.

Equation (9) makes sense when $d < g$. Consequently, when plasma density exceeds n_0 with

$$n_0 = 2\epsilon_0 V_g / e g^2 = 1.1 \times 10^9 \text{ cm}^{-3} \left(\frac{V_g}{1 \text{ kV}} \right) \left(\frac{1 \text{ cm}}{g} \right)^2, \quad (10)$$

rf sheath effects close the gap and raise the electric field at the plasma-screen boundary to a value

$$E = \left(\frac{2neV_g}{\epsilon_0} \right)^{1/2} = \left(6 \frac{\text{kV}}{\text{cm}} \right) \left(\frac{n}{10^{10} \text{ cm}^{-3}} \frac{V_g}{1 \text{ kV}} \right)^{1/2}, \quad (11)$$

which significantly exceeds a representative value of $E \sim 1 \text{ kV/cm}$ in the absence of a plasma.

Will this intense electric field cause sputtering? The energy U_i obtained by an unmagnetized ion starting from rest at the plasma-screen boundary in one-half wave period is

$$U_i = \frac{2e^2 E^2}{M\omega^2} = (eV_g) \frac{4\nu_{pi}^2}{\nu^2}, \quad (12)$$

where ν_{pi} is the deuterium ion plasma frequency

$$\nu_{pi} = \frac{1}{2\pi} \left(\frac{ne^2}{M\epsilon_0} \right)^{1/2} = 16 \text{ MHz} \left(\frac{n}{10^{10} \text{ cm}^{-3}} \right)^{1/2}. \quad (13)$$

In most ICRF heating experiments, one expects that the plasma density in the gap between Faraday screen elements will be sufficiently high so that

$n > n_0$ and $\nu \lesssim 2\nu_{pi}$. Estimate (12) then shows that the ion energy is comparable to the potential drop across the gap and lies near the maximum of the physical sputtering yield curves [16-18].

One can now check, *a posteriori*, the validity of the immobile ion assumption. The distance moved by an unmagnetized ion in half a wave period is

$$\Delta x = \frac{eE\pi}{M\omega^2}, \quad (14)$$

and using Eq. (8), one finds

$$\frac{\Delta x}{d} = \frac{\pi\nu_{pi}^2}{\nu^2} + O(1). \quad (15)$$

Thus an ion traverses the space charge region in half a wave period and an immobile ion model is just at its limit of validity. Estimate (12) for the energy gained by an ion remains qualitatively correct, but additional factors of order unity are expected.

The next section develops a one-dimensional Vlasov model for rf sheaths. Since the principal physical effect developed in this section – gap closure by electron motion along magnetic field lines – is a one-dimensional effect, we expect the qualitative aspects of this work to persist along all field lines which join two Faraday screen elements.

3. ONE-DIMENSIONAL RF SHEATHS

Computational studies of time-dependent plasma sheaths surrounding driven objects are just beginning. A recent paper by Borovsky [24] deals

with one-dimensional models of abrupt spacecraft charging, and provides extensive references to the literature. This work is similar to that of Borovsky in that driving voltages appreciably exceed ambient plasma temperatures. But it is the asymptotic response to a.c. driving voltages, not transients, that is important for ICRF applications.

The simplest model for rf sheath effects is based on one-dimensional geometry and unmagnetized ions. Mathematically, it corresponds to a 2-dimensional phase-space (y, v_y) . Physically, its justification rests on three criteria. First, the potential drop across the gap should not vary appreciably over the distance along the gap which a magnetic field line travels while traversing the gap, i.e., $l \gg g/\theta$ where l denotes the length of a Faraday screen element, g the gap width, and θ the misalignment angle. This criterion is fulfilled for many current Faraday screen designs. The second criterion is that fringing field effects associated with the real 2-dimensional geometry of Faraday screen elements be small. If the space charge region thickness d defined in Eq. (9) is small compared to the gap width, one expects 2-dimensional geometry effects to be small. Hence, by Eq. (10), this criterion will be fulfilled provided the gap density n satisfies $n \gg n_0 = 2\epsilon_0 V/eg^2 = 1.1 \times 10^9 \text{ cm}^{-3} (V/1 \text{ kV})(1 \text{ cm/g})^2$ – in accord with reasonable estimates of the gap density. The third criterion is that ion motion be effectively unmagnetized. This means that $\omega \gg \Omega_i$, a condition only marginally fulfilled in practice. Furthermore, as Fig. 2 makes clear, rf sheaths produce a rectification effect; on one half cycle, the electric field in the space region near the boundary is intense and pointed towards the boundary, while

in the second half cycle electron shielding reduces the electric field. Hence, there is a strong time-averaged field seen by the ions. In an unmagnetized ion model, this accelerates all ions in the gap towards the nearest wall, while in a magnetized ion model, $\mathbf{E} \times \mathbf{B}$ drifts would result. For an ion accelerated to the gap potential, one can estimate that the ratio of ion gyroradius ρ_i to sheath thickness is

$$\frac{\rho_i^2}{d^2} = \frac{2eV}{Md^2\Omega_i^2} = \frac{\omega_{pi}^2}{\Omega_i^2} \sim 0(1), \quad (16)$$

where (10) was used to eliminate d . Thus, for ions in the space charge region, magnetic effects are important but not overwhelming. Qualitatively, an unmagnetized ion model should provide useful estimates of rf sheaths, and this assumption simplifies the mathematical model from 3-dimensional (y, v_x, v_y) to 2-dimensional (y, v_y) .

Our model does not address how plasma gets into a Faraday screen gap; we simply assume that a certain density exists and introduce a source term into the Vlasov equation to maintain a fixed ion content in the gap region. The electron content is permitted to vary so that Debye-length sheaths, which regulate electron losses, can be established near the positive boundary.

The Vlasov equations which correspond to the gap lying in the interval $0 \leq y \leq g$ are

$$\frac{\partial F}{\partial t} + v_y \frac{\partial F}{\partial y} - \frac{eE_y}{m^*} \frac{\partial F}{\partial v_y} = S \left(\frac{m^*}{2\pi T_e} \right)^{1/2} \exp \left(\frac{-m^* v_y^2}{2T_e} \right), \quad (17)$$

$$\frac{\partial G}{\partial t} + u_y \frac{\partial G}{\partial y} + \frac{eE_y}{M_i} \frac{\partial G}{\partial u_y} = S \left(\frac{M_i}{2\pi T_i} \right)^{1/2} \exp \left(\frac{-M_i v_y^2}{2T_i} \right), \quad (18)$$

$$S = S_0 \left[1 - \cos \left(\frac{2\pi y}{g} \right) \right], \quad (19)$$

$$S_0 = - \int_{\infty}^0 du_y u_y G(0, u_y) + \int_0^{\infty} du_y u_y G(g, u_y), \quad (20)$$

$$E_y = -\frac{\partial \Phi}{\partial y} = -\frac{V_g(t)}{g} + \int_0^y \rho(y') dy' - \int_0^g \left(1 - \frac{y'}{g}\right) \rho(y') dy', \quad (21)$$

$$\rho(y) = (e/\epsilon_0) \left[\int_{-\infty}^{\infty} G du_y - \int_{-\infty}^{\infty} F dv_y \right]. \quad (22)$$

Expression (21) corresponds to a solution to Poisson's equation where the voltage rise across the gap is $V_g(t)$. The source terms (19)–(20) replace plasma according to the rate at which ions strike the walls. The source spatial distribution (19) is purely ad hoc, but physically motivated by the principle that plasma is advected into the center of the gap, rather than along the walls. It will require at least a 4-dimensional model (x, y, v_x, v_y) to investigate the nature of the plasma source.

Next, let us recast these equations into a nondimensional form, using

$$\xi = y/g, \quad \tau = \omega_0 t, \quad v = v_y/\omega_0 g, \quad (23)$$

$$\omega_0 = (n_0 e^2 / m^* \epsilon_0)^{1/2} \quad u = u_y/\omega_0 g, \quad (24)$$

$$M = M_i/m^* \quad E = -E_y \epsilon_0 / n_0 e g = \partial \phi / \partial \xi, \quad (25)$$

$$V = V_g \epsilon_0 / n_0 e g^2 \quad \phi = \Phi \epsilon_0 / n_0 e g^2, \quad (26)$$

$$f = F \omega_0 g / n_0 \quad h = G \omega_0 g / n_0, \quad (27)$$

where n_0 denotes the average electron density in the gap region. The nondimensional equations are

$$\frac{\partial f}{\partial \tau} + u \frac{\partial f}{\partial \xi} + E \frac{\partial f}{\partial u} = \sigma \frac{1}{\sqrt{\pi} u_0} e^{-u^2/u_0^2}, \quad (28)$$

$$\frac{\partial h}{\partial \tau} + v \frac{\partial h}{\partial \xi} - \frac{E}{M} \frac{\partial h}{\partial v} = \sigma \frac{1}{\sqrt{\pi} v_0} e^{-v^2/v_0^2}, \quad (29)$$

$$\sigma = \sigma_0[1 - \cos(2\pi\xi)], \quad (30)$$

$$\sigma_0 = - \int_{-\infty}^0 du \, u h(0, u) + \int_0^{\infty} du \, u h(1, u), \quad (31)$$

$$E = V(t) - \int_0^{\xi} \rho(\xi') d\xi' + \int_0^1 (1 - \xi') \rho(\xi') d\xi', \quad (32)$$

$$\rho(\xi) = \int_{-\infty}^{\infty} h dv - \int_{-\infty}^{\infty} f du, \quad (33)$$

$$V(t) = V_0 \sin(\omega\tau)[1 - \exp(-\frac{\omega\tau}{5})] \quad (34)$$

$$M = M_i \theta^2 / m_e.$$

Equation (34) for the gap voltage was chosen to suppress transients associated with a rapid switch-on of the rf voltage. The boundary conditions for the Vlasov equation at the material surfaces ($\xi = 0, \xi = 1$) are that impinging particles are absorbed and no particles are emitted. A volume source term σ maintains the ion content constant.

Equations (28-34) were solved computationally for two representative cases given in Table I. A (ξ, u) phase space fluid representation conserved energy to better than 0.5% after 8 periods of the impressed wave form (34).

Figures 3 and 4 present the key results: the energy and flux of ions impacting on the material boundaries. Ion energies typically lie in the range 500-700 eV, certainly adequate for physical sputtering. Figures 5 and 6 show electron and ion densities as well as the potential when the impressed voltage is at its maximum. It is clear that the qualitative features of rf sheaths illustrated in Fig. 2 are realized in the computational solutions. Fine scale structure is numerical. Rectified electric fields give ions near the boundaries a high degree of directed kinetic energy towards the nearer boundary. In a

magnetized ion model, this velocity would become cyclotron motion. Hence, the present unmagnetized model overestimates the flux impacting on boundaries, especially for low density plasmas ($n \lesssim 10^{11}\text{cm}^{-3}$), where Eq. (16) shows that the rf sheath thickness is comparable to or greater than the gyroradius. Conversely, the overestimate should not be severe for gap plasma densities exceeding $n \sim 10^{11}\text{cm}^{-3}$.

Can sputtering account for the observed metallic impurity influx? Behring er *et al.* [9] report the impurity flux to be $\sim 10^{16}\text{atoms/cm}^2\text{-sec MW}$. The results of Figs. 3 and 4, recast in dimensional units, correspond to impacting ion fluxes of

$$F \approx \begin{cases} 7.0 \times 10^{16}\text{cm}^{-2}\text{sec}^{-1} & n = 10^{10}\text{cm}^{-3} \\ 2.3 \times 10^{17}\text{cm}^{-2}\text{sec}^{-1} & n = 10^{11}\text{cm}^{-3}. \end{cases} \quad (35)$$

The average flux Φ of metallic impurities is then

$$\Phi = FY\eta \approx 10^{-2}F, \quad (36)$$

where $Y \approx 0.04\text{ atoms/ion}$ is the sputtering yield for deuterium incident on nickel at an energy of 500 eV [17] and η denotes the fraction of the surface where sputtering occurs. An ad hoc estimate is $\eta \approx 0.25$. One concludes that, if plasma densities exceed $n = 10^{11}\text{cm}^{-3}$, sputtering by ions accelerated in an rf sheath could reasonably account for the observed influx. Since our model takes plasma density as a parameter, there is no way to estimate how n and, consequently, sputtering flux, scales with power.

Our computational solutions also showed significant electron heating with T_e increasing from 25 eV to 70 eV, and spontaneous generation of plasma

waves. Figure 7 shows representative potential, electron density, and ion density profiles clearly exhibiting plasma waves, which were quite evident in cinema displays of results. Plasma waves were most intense during periods of maximum electron velocity when electrons were sloshing from one side of the gap to the other. The specifics of these waves —frequency, wavelength, etc. —may well be particular to 1-dimensional geometry, but their appearance suggests placing plasma wave and electron temperature diagnostic probes in Faraday screen slots.

4. ICRF ANTENNA DESIGN

The key results of this paper are conceptual: First, arguments based on data conclude that ICRF-induced hydrogen and carbon influx is a global phenomenon, dependent on the presence of fast Alfvén waves, but not on the particulars of antenna design. Secondly, numerical calculations show that metallic impurity generation takes place near sheaths which occur when magnetic field lines traverse from one Faraday screen element to the next. This conceptual picture immediately suggests three classes of improvements for ICRF antenna design: 1) Align Faraday screen elements along the magnetic field. 2) Orient surfaces where sputtering occurs to emit impurities away from the plasma. 3) Coat Faraday screen elements with low- Z material so that the sputtered material does not radiate severely at high temperatures. Step 3) is already being taken in present ICRF antennas [13]. Step 1) calls for an antenna whose screen element orientation is continuously variable. Figure 8 sketches a rotating antenna configuration. Such designs have

not been attempted, largely because TFR experiments [21] indicated the expected benefits to be minimal. The conceptual picture of this paper, coupled with recent JET data [20], suggests that benefits may be appreciable. At the very least, screen element orientation is one of the parameters that can be chosen by machine designers, and experimental antennas to explore this parameter are warranted.

If the hypothesis that metallic impurity generation takes place preferentially at those surfaces of Faraday screen elements which intersect magnetic field lines is correct, then it is possible to design screen elements so that these surfaces face away from the plasma. Since sputtered atoms are emitted principally normal to the surface [17], most of the sputtered atoms will not enter the plasma. Figure 9 sketches a heuristic design. Note that the screen elements on the two rows are sufficiently separated so that magnetic field lines do not connect elements on different rows.

The key hypothesis of this work is that ICRF-induced impurity generation has two sources: 1) that coming from the Faraday screen and 2) a global influx associated with the presence of ICRF waves in a tokamak. The physics of the second source is outside the scope of this paper.

This paper concludes that rf sheaths near Faraday screen elements constitute the key physics of the first source and the only one affected by antenna power density. Improved antenna design might well eliminate this source, permitting antenna power densities to reach 10 kW/cm^2 . Definitive answers must rest on an experimental program of innovative antenna design and plasma diagnostic probes placed in the Faraday screen gap.

ACKNOWLEDGMENT

This work is supported by U.S. Department of Energy Contract No. DE-AC02-76-CHO3073.

References

- [1] SCHMIDT, J., BATEMAN, G., BUSHNELL, C., *et al.*, in *Plasma Physics and Controlled Nuclear Fusion Research 1986* (Proc. 11th. Int. Conf. Kyoto, 1986) Vol. 3, IAEA, Vienna (1987) 259.
- [2] ADAM, J., *Plasma Phys. Controll. Fusion* **29** (1987) 443.
- [3] MAZZUCATO, E., BELL, R., BITTER, M., *et al.*, in *Plasma Physics and Controlled Nuclear Fusion Research 1984* (Proc. 10th. Int. Conf., London, 1984) Vol.1, IAEA, Vienna (1985) 433.
- [4] LALLIA, P.P., JET TEAM, *Plasma Phys. Controll. Fusion* **28** (1986) 1211.
- [5] WOLF, G.H., BAY, H.L., BERTSCHINGER, G., *Plasma Phys. Controll. Fusion* **28** (1986) 1413.
- [6] STEINMETZ, K., SÖLDER, F.X., ECKHART, D., *et al.*, in *Plasma Physics and Controlled Nuclear Fusion Research 1986* (Proc 11th Int. Conf. Kyoto, 1986) Vol.1, IAEA Vienna (1979) 461.
- [7] BAITY, F.W., SWAIN, D.W., HOFFMAN, D.J., Proc. 14th. Symp. Fusion Technology (Avignon, 1986) 743.
- [8] MANNING, H.L., TERRY, J.L., LIPSCHULTZ, B. *et al.*, *Nucl. Fusion* **26** (1986) 1665.

- [9] BEHRINGER, K., BOILEAU, A., BOMBARDA, F., *et al.*, in *Plasma Physics and Controlled Nuclear Fusion Research 1986* (Proc. 11th Int. Conf., Kyoto, 1986) Vol.1, IAEA, Vienna (1987) 197.
- [10] ENGELHARDT, W.W., JET TEAM, *Plasma Phys. Controll. Fusion* **28** (1986) 1401.
- [11] ERENTS S.K., TAGLE, J.A., McCACKEN, G.M. *et al.* *J. Nucl. Materials* **143-145** (1987) 231.
- [12] PERKINS, F.W., KLUGE, R.F., *IEEE Trans. Plasma Sci.* **PS-12** (1984) 161.
- [13] HOFFMAN, D.J., COLESTOCK, P.L., GARDNER, W.L., in *Proc. 15th European Conf. Controlled Fusion and Plasma Heating*, Contributed Papers, Vol.2 (European Physical Society, Dubrovnik, 1988) 770.
- [14] BRINKSCHULTE, H., CLEMENT, S., COAD, J.P., in *Proc. 15th. European Conf. Controlled Fusion and Plasma Heating*, Contributed Papers, Vol.2 (European Physical Society, Dubrovnik, 1988) 659.
- [15] BEHRINGER, K.H., *J. Nucl. Materials* **145-147** (1987) 145.
- [16] ROTH, J. in *Physics of Plasma-Wall Interactions in Controlled Fusion* Ed. D. Post and R. Behrisch (Plenum Press, New York, 1986) 351.
- [17] LANGLEY, R.A., BONDASKY, J., ECKSTEIN, W. *et al.*, *Data Compendium for Plasma-Surface Interactions*, *Nucl. Fusion*, Special Issue (IAEA, 1984)

- [18] ROTH, J., J. Nucl. Materials **145-147** (1987) 87.
- [19] CAUGMAN, J.B.O. II, RUZIC, D.N., HOFFMAN, D.J., J. Vac. Sci. Technol. **A5** (1987) 2301.
- [20] BURES, M., BHATNAGER, V., CORTI, S. *et al.*, Proc. 15th. European Conf. Controlled Fusion and Plasma Heating, Contributed Papers, Vol.2 (European Physical Society, Dubrovnik, 1988) 713.
- [21] TFR GROUP, SAND, F., Nucl. Fusion **25** (1985) 1719.
- [22] PERKINS, F.W. in *Proc. 4th. Int. Symp. Heating in Toroidal Plasmas*, Ed. H.Knoepfel and E. Sindoni, Vol.2 (International School of Plasma Physics, Rome, 1984) 1148.
- [23] FAULCONER, D.W. in *Proc. 4th. Int. Symp. Heating in Toroidal Plasmas*, Ed. H. Knoepfel and E. Sindoni, Vol.2 (International School of Plasma Physics, Rome, 1984) 1157.
- [24] BOROVSKY, J.E., Phys. Fluids **31** (1988) 1074.

Table

Table I. Parameters for Computational Solutions.

Parameter	I	II
Physical Parameters		
gap density n_0	10^{10}cm^{-3}	10^{11}cm^{-3}
gap width g	1 cm	1 cm
gap voltage V_g	900 V	900 V
electron temperature	23 eV	28 eV
ion temperature	9 eV	11 eV
misalignment angle (rad)	0.1	0.1
effective plasma frequency	90 MHz	284 MHz
impressed rf frequency	45 MHz	45 MHz
Nondimensional Parameters		
ω	0.5	0.158
V_0	0.05	0.005
u_0	0.05	0.0175
v_0	0.005	0.00175
M	40.0	40.0

Figures

FIG. 1. Faraday screen geometry. a) Almost all the rf magnetic field lines which encircle the driven current strap pass twice through gaps of width g and length l between screen elements. b) Typical Faraday screen elements run along the purely toroidal direction \hat{z} , and cross the combined poloidal and toroidal field at an angle θ . c) RF magnetic flux which penetrates through one side of the slot must return through the other. ABCD refers to Eq. (3).

FIG. 2. Electron density, ion density, and potential in an immobile ion model [(cf. Eqs. (8-15))].

FIG. 3. Normalized flux and ion impact energy for the low density case $n = 10^{10} \text{ cm}^{-3}$. a) Normalized flux versus time in impressed wave periods. Flux is normalized to a value of $5.6 \times 10^{18} \text{ cm}^{-2} \text{ sec}^{-1}$. b) Ion impact energy normalized to a value of 900 eV.

FIG. 4. Normalized flux and ion impact energy for the high density case $n = 10^{11} \text{ cm}^{-3}$. a) Normalized flux versus time in impressed wave periods. Flux is normalized to a value of $1.8 \times 10^{20} \text{ cm}^{-2} \text{ sec}^{-1}$. b) Ion impact energy normalized to a value of 900 eV.

FIG. 5. Representative electron and ion densities and potential (in units of 18 kV) versus position for case I of Table I. Fine scale structure is numerical.

FIG. 6. Representative electron and ion densities and potential (in units of 180kV) versus position for case II of Table I. Fine scale structure is numerical.

FIG. 7. Representative electron and ion densities and potential (in units of 180kV) versus position for case II of Table I. The time has been selected to show maximum plasma wave amplitudes.

FIG. 8. Rotating antenna configuration. A conducting box containing the driven element as well as the Faraday screen rotates within a rectangular port. Most of the port area is utilized for the antenna. Magnetic loop coupling from coaxial transmission lines at a non-rotating backwall (cf [12]) could be used.

FIG. 9. Faraday screen elements designed so that those surfaces which are connected by poloidal field are oriented to direct sputtering atoms away from the plasma.

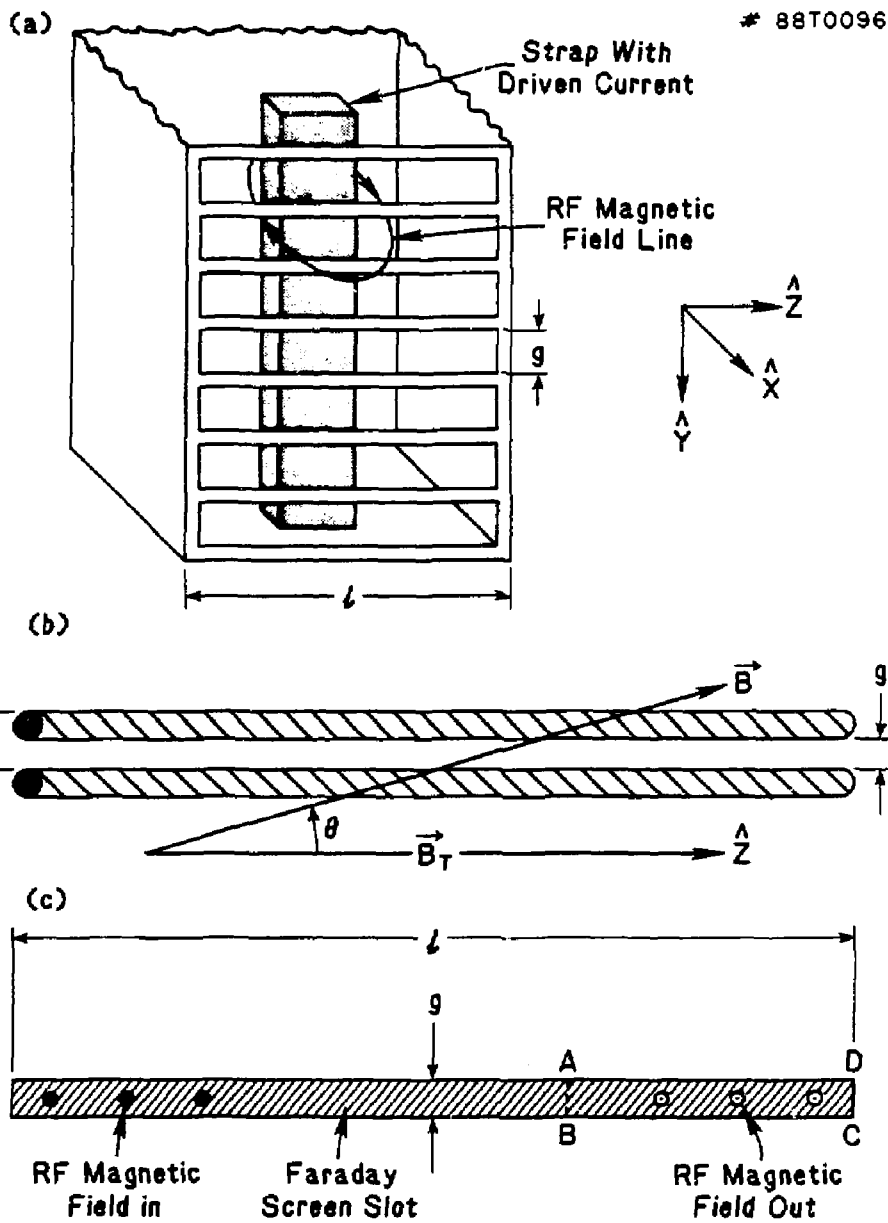


Fig. 1

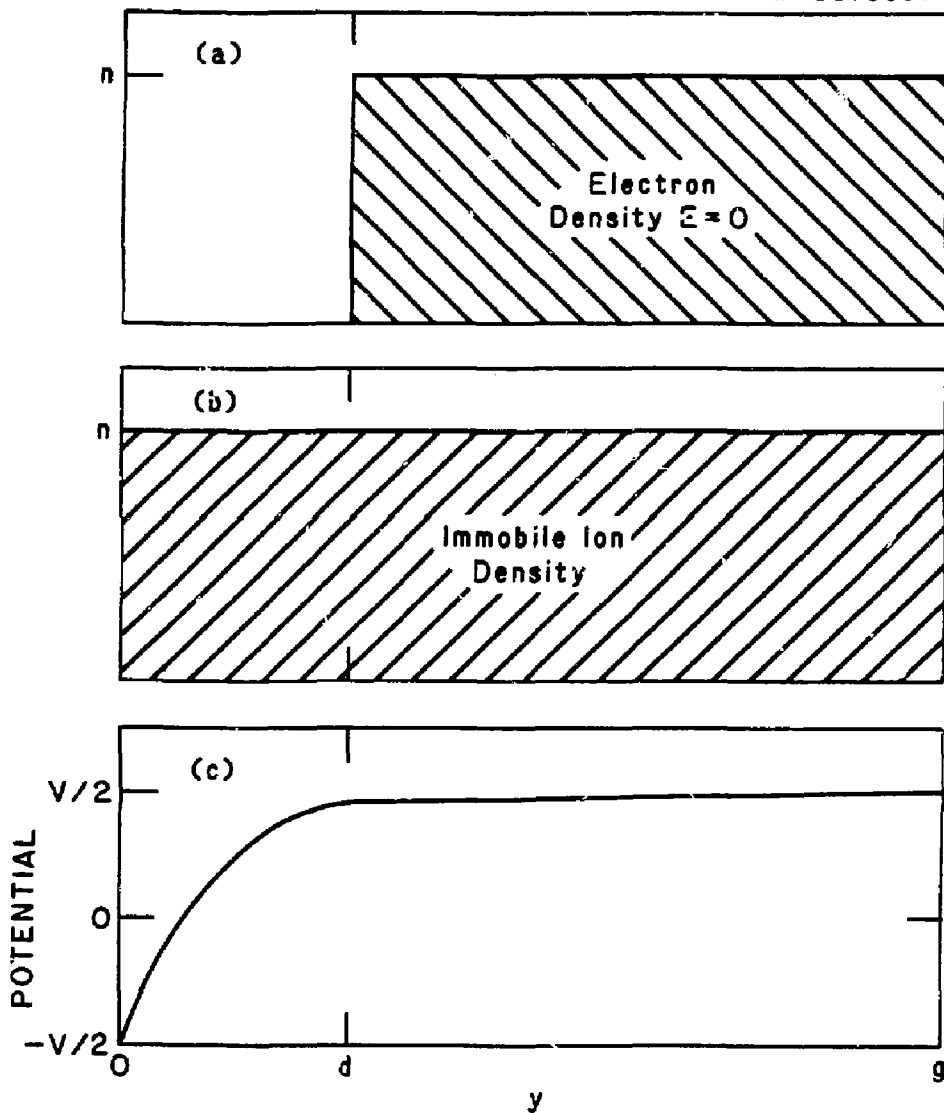


Fig. 2

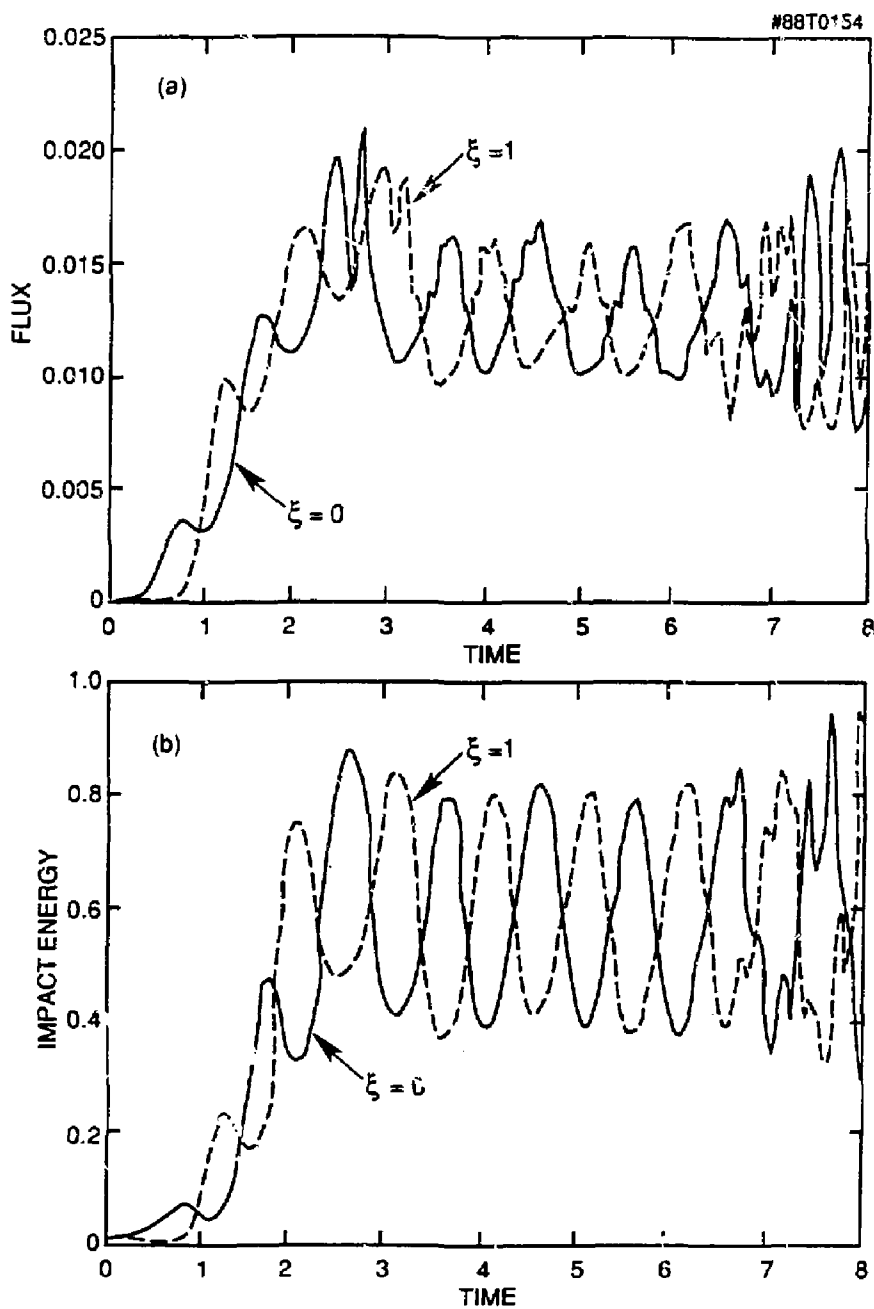


FIG. 3

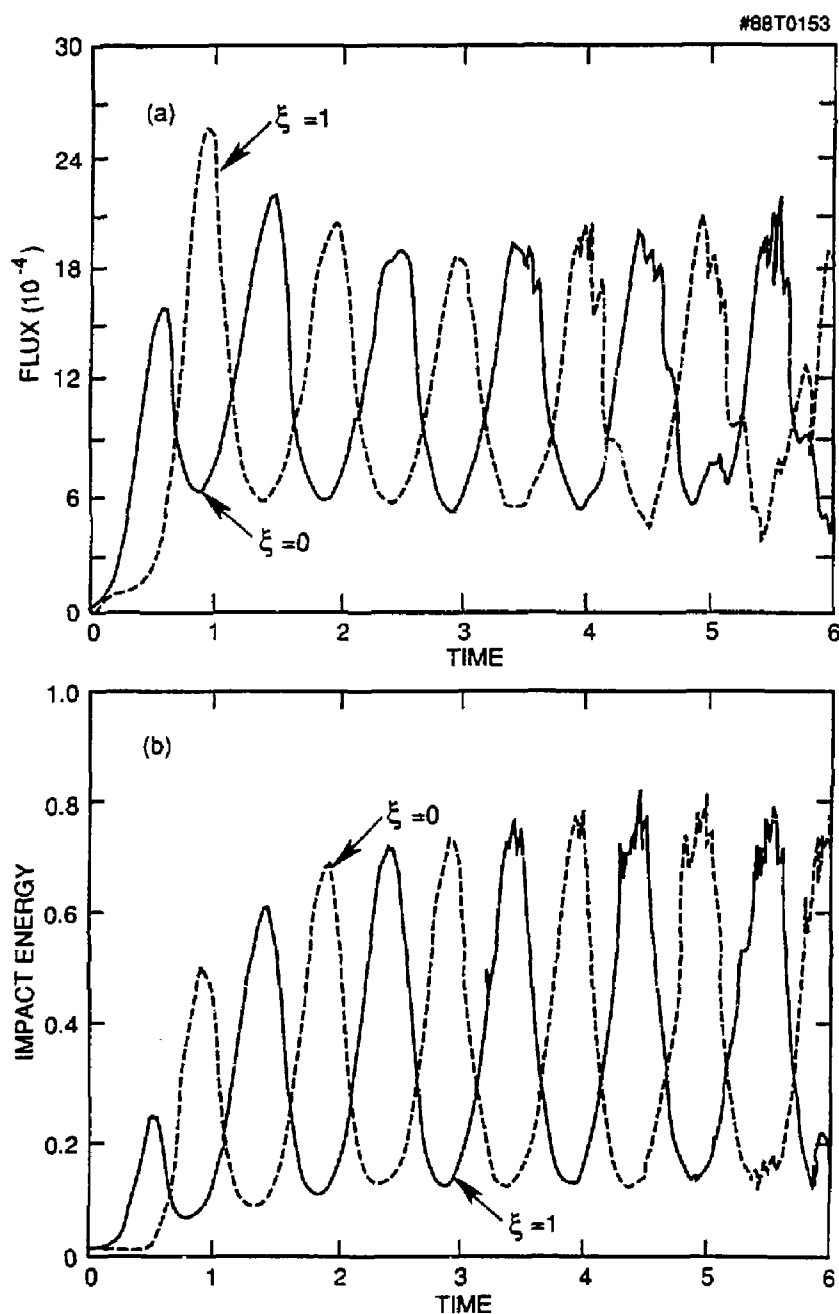


FIG. 4

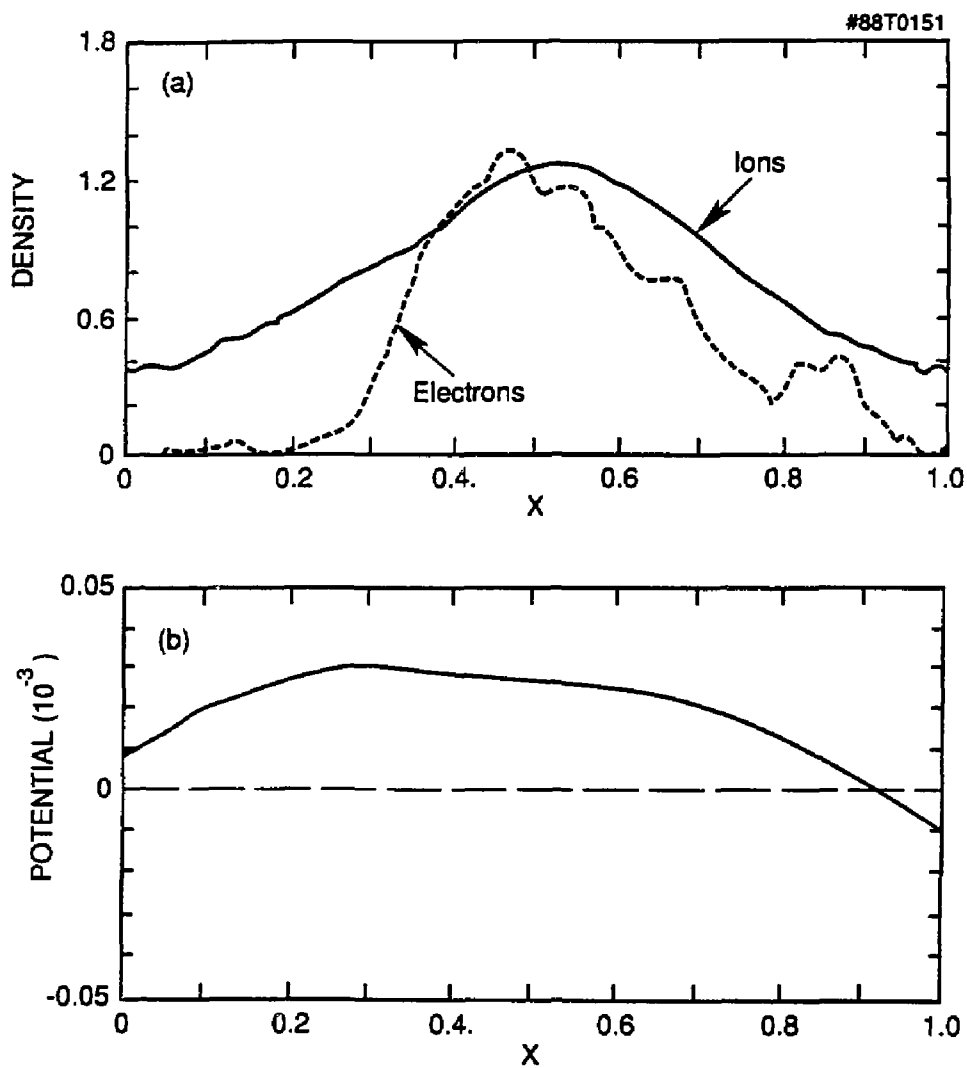


Fig. 5

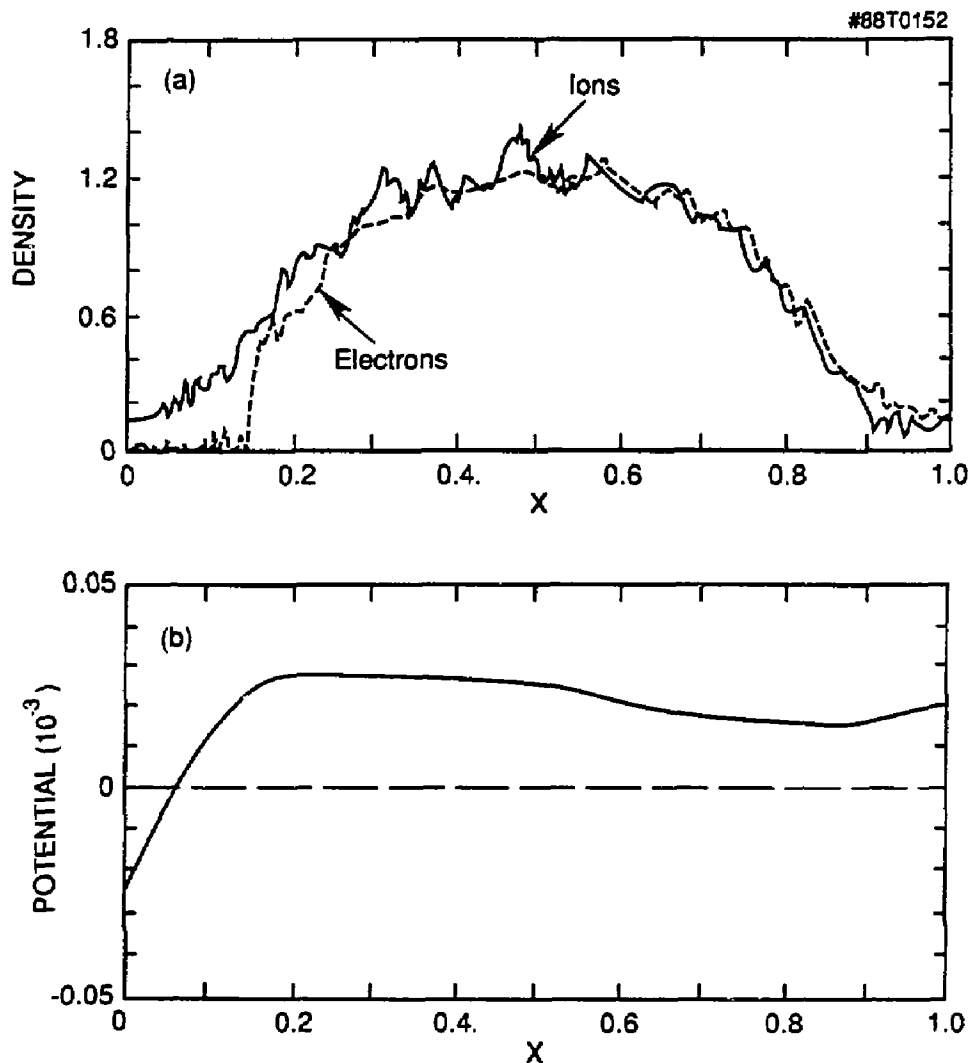


FIG. 6

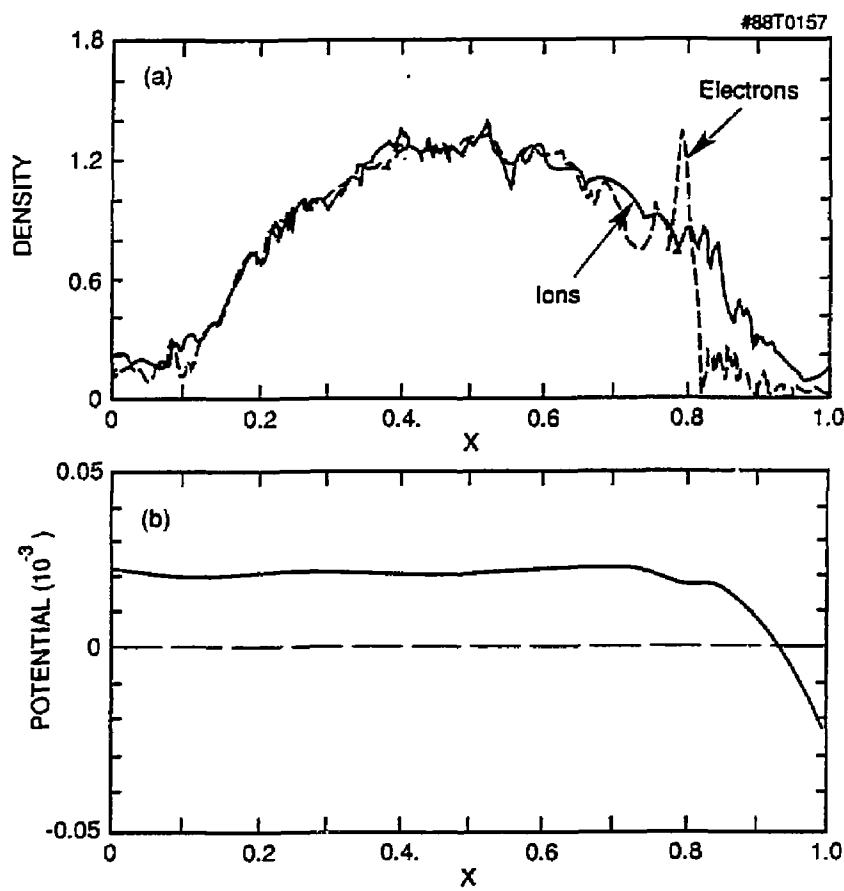


FIG. 7

#88T0150

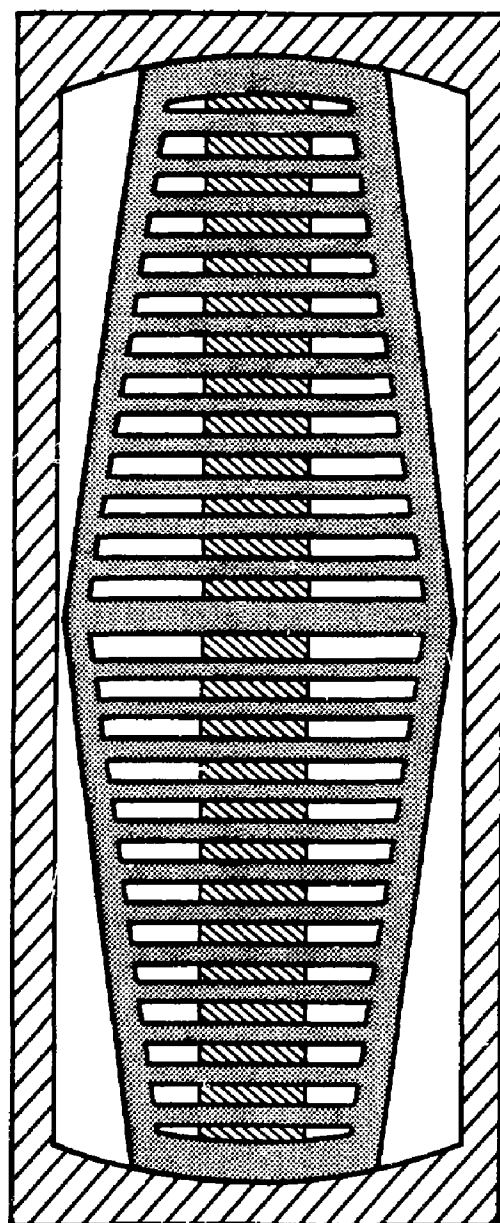


FIG. 8

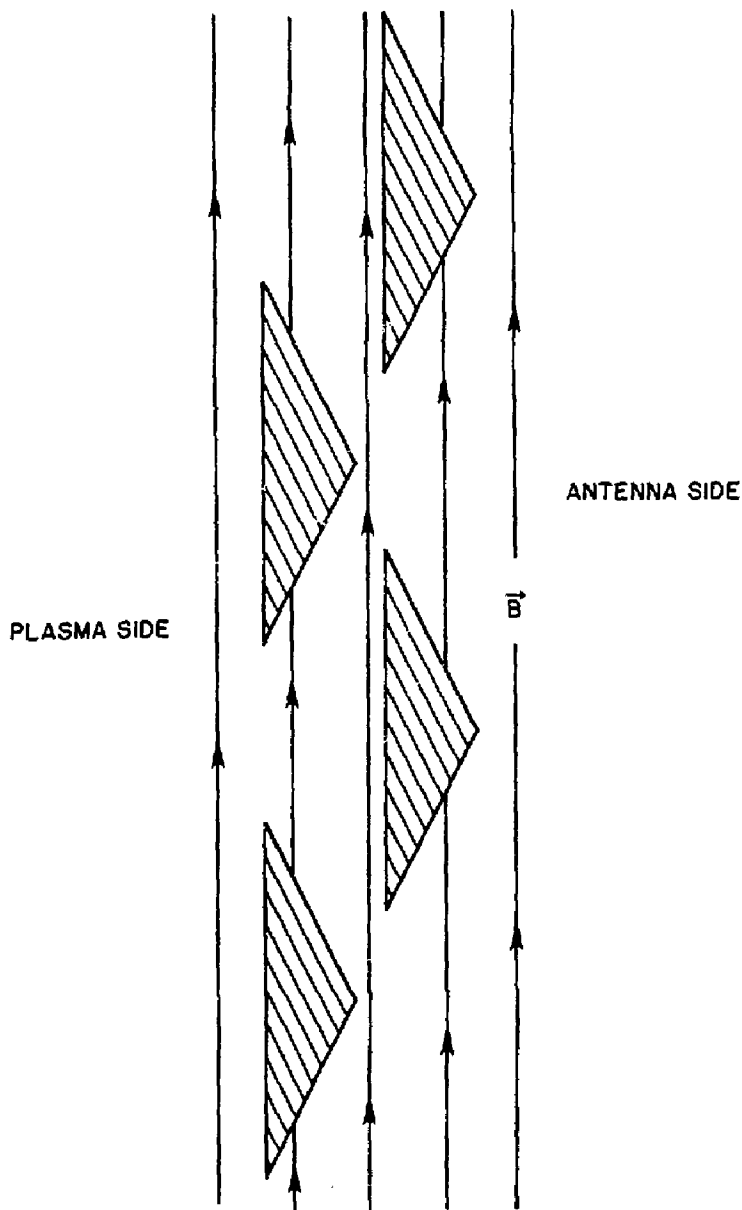


FIG. 9